

CrossMark
click for updatesCite this: *J. Mater. Chem. A*, 2014, 2, 18929

Hollow nickel-coated silica microspheres containing rhodium nanoparticles for highly selective production of hydrogen from hydrous hydrazine†

Jung Bo Yoo, Han Sol Kim, Seung Hee Kang, Byeongno Lee and Nam Hwi Hur*

The synthesis of hollow nickel-coated silica microspheres containing rhodium nanoparticles (NPs) (Rh/Ni@SiO₂) via thermal hydrolysis of urea using core-shell silica microspheres as templates is described. This dissolution-and-deposition method using urea as a precipitating agent provided uniform hollow microspheres composed of amorphous Ni(OH)₂ and silica (SiO₂) layers along with small amounts of Rh species even without etching; these hollow microspheres transformed to crystalline Rh/Ni@SiO₂ microspheres after annealing at 750 °C under a reducing atmosphere. The formation of a hollow structure is dependent on the concentration of urea and unique dissolution behavior of the core-shell silica. The bimetallic Rh/Ni@SiO₂ microsphere with a low Rh content (6.35 wt%) is a highly active catalyst for complete dissociation of hydrous hydrazine into hydrogen and nitrogen. Complete release of hydrogen from hydrous hydrazine was accomplished at 25 °C with a H₂ selectivity of 99.4% and turnover number of 66. The used Rh/Ni@SiO₂ catalyst, which was recovered by a magnet, was reused in subsequent reactions with virtually identical activity.

Received 11th July 2014
Accepted 16th September 2014

DOI: 10.1039/c4ta03550j

www.rsc.org/MaterialsA

Introduction

Combustion of fossil fuels produces large amounts of carbon dioxide (CO₂), which is a main contributor to climate change. In contrast, hydrogen (H₂) is free of carbon and its combustion produces water as the only waste product. Accordingly, hydrogen plays a major role in the generation of clean energy and reduction of CO₂ emissions.^{1–3} However, a major drawback is that hydrogen is very difficult to store and transport because it exists as a flammable gas under ambient conditions. An alternative approach is to develop hydrogen storage materials that satisfy several technical requirements, including sufficiently high volumetric and gravimetric capacities, facile release of hydrogen at a reasonably low temperature, and efficient regeneration at a practical temperature.⁴ Thus far, a wide range of hydrogen storage materials, such as nano materials,⁵ metal hydrides,⁶ chemical hydrides,⁷ and liquid organic compounds,⁸ has been explored to facilitate the use of hydrogen as a fuel. In particular, chemical hydrides composed of boron, nitrogen, and hydrogen atoms have drawn significant interest because they are light atoms with high gravimetric hydrogen capacities. In addition, hydridic B–H and protic N–H bonds can thermally or

catalytically dissociate to yield hydrogen. Numerous boron-nitrogen compounds have been evaluated as potential hydrogen-storage materials; they are suitable for producing hydrogen under relatively mild conditions but yield undesired products that cannot be regenerated by hydrogenation under practical conditions.^{9–15}

On the other hand, liquid organic hydrogen-storage materials possess significant advantages over solid hydrides,⁸ particularly in on-board applications, because they can be handled like fuel in a vehicle. After releasing hydrogen, the dehydrogenated materials can be regenerated by hydrogenation or stored in another tank. However, most of these reversible organic compounds have low gravimetric capacities and require significant energy to dissociate the C–H and N–H bonds. Anhydrous hydrazine (H₂NNH₂) is a promising hydrogen storage material because it has a high H₂ content (12.5 wt%) and is in the liquid state at room temperature. Moreover, it can ideally be dissociated into hydrogen and nitrogen.¹⁶ However, direct use of anhydrous hydrazine is restricted because it is extremely toxic, highly reactive, and even explosive. Hydrous hydrazine, which is prepared by diluting hydrazine with water, is thus used as an alternative to mitigate the toxicity and reactivity of anhydrous hydrazine.^{17–20} Complete decomposition of hydrazine yields only hydrogen and nitrogen according to the following equation: H₂NNH₂ → N₂ (g) + 2H₂ (g). Hydrazine can also incompletely decompose into ammonia and nitrogen, as follows: 3H₂NNH₂ → 4NH₃ (g) + N₂ (g). The dissociation

Department of Chemistry, Sogang University, Seoul 121-742, Korea. E-mail: nhhur@sogang.ac.kr

† Electronic supplementary information (ESI) available. See DOI: 10.1039/c4ta03550j

pathways depend significantly on the catalyst and reaction conditions. A wide range of catalysts based mostly on metal nanoparticles (NPs) have been developed for complete decomposition of hydrous hydrazine.^{21–28} Rh NPs have proven to be very active for the production of H₂ from hydrous hydrazine: their H₂ selectivity is close to 43%.²⁹ Monometallic catalysts containing Co, Ru, or Ir NPs are also active for the decomposition reaction but their selectivity is very low (<7%). Most Ni-based bimetallic catalysts with precious metals show enhanced selectivity towards H₂ production;^{30–35} their activities not only depend on the metal composition but also on the compositional ratio. Thus far, an Rh-rich alloy (*i.e.*, Rh₄Ni) shows the highest selectivity (~100%) for the production of H₂ from hydrous hydrazine at room-temperature.³⁵ However, complete replacement of Rh by abundant metals or reduction of the Rh content by alloying with inexpensive metals is necessary for this technology for producing H₂ from hydrazine to be industrially viable.^{36–38}

Thus far, most of the catalysts developed for complete decomposition of hydrous hydrazine are NPs that are typically composed of noble metals and transition metals. Bimetallic NPs have a high surface area, which is very advantageous, particularly for catalytic activity. The synthesis of bimetallic NPs typically requires high temperatures, which lead to agglomeration of the NPs. To prevent aggregation, NPs can be covered with capping agents; however, these often hamper the catalytic reaction. Another drawback is that bimetallic NPs are difficult to separate and reuse in a subsequent reaction mainly because of their extremely small sizes. From this perspective, hollow microspheres containing active-metal NPs on their outer surfaces are significant challenges both synthetically and catalytically. An important benefit of hollow microspheres is that they can be used as recyclable supports with high surface areas.

Hollow materials containing metal NPs are typically prepared using sacrificial templates.^{39–41} This process involves coating the desired materials onto the templates and then etching the templates away to form the hollow structure. In previous work, we prepared hollow materials through selective etching of the templates using a concentrated alkaline solution.⁴² This methodology is simple but partially degrades the active shell components. The reports on the syntheses of hollow materials without etching have thus far been limited. In the present work, we use core-shell silica (SiO₂) microspheres as templates and employ urea as an alkaline medium, thereby forming hollow microspheres that contain metal species without etching. This dissolution-and-deposition method proceeds through thermal hydrolysis of urea. Urea is a simple organic compound that has two NH₂ groups connected by a carbonyl (CO) group; it is neither acidic nor alkaline in water under ambient conditions. Upon heating, however, it produces ammonia in water, which causes the solution to become alkaline. A urea solution at high temperature can dissolve silica in a controlled manner even though it is only slightly soluble.^{43–52} The weak alkalinity of the urea solution leads to the uniform deposition of metal precursors and gradual dissolution of the silica core.

Herein, we report hollow nickel-coated microspheres containing Rh NPs (Rh/Ni@SiO₂) that were prepared by thermal hydrolysis of urea using core-shell silica microspheres as templates followed by annealing at 750 °C under flowing 5% H₂ in an Ar atmosphere. The Rh/Ni@SiO₂ microspheres maintain a spherical shape, have large cavities in the core, and contain less than 6.35 wt% Rh. At room temperature, the Rh/Ni@SiO₂ catalyst generates H₂ with over 99% selectivity within 1.5 h. Moreover, the used Rh/Ni@SiO₂ catalyst recovered by a magnet produces H₂ at the same selectivity; these results generate significant promise for hydrous hydrazine as a potential hydrogen-storage material.

Experimental section

Chemicals

All chemicals were purchased from commercial suppliers and used without further purification unless otherwise stated. Tetraethyl orthosilicate (TEOS), nickel acetylacetonate (C₁₀H₁₄NiO₄), and rhodium chloride hydrate (RhCl₃·xH₂O) were purchased from Tokyo Chemical Industry Co. (Tokyo, Japan). Octadecyl trimethoxysilane (C₁₈-TMS), hydrazine hydrate (H₂NNH₂·H₂O, 98%), benzyl aldehyde, phenol, sodium hypochlorite (NaOCl), sodium hydroxide (NaOH), sodium nitroferricyanide dihydrate (Na₂[Fe(CN)₅NO]·2H₂O), and urea were purchased from Sigma-Aldrich (St Louis, USA). Ethanol, deionized water, sulfuric acid, and ammonia solution (25–28%) were obtained from Samchun Chemical Reagent Co. (Seoul, Korea).

Synthesis of core-shell silica microspheres (core-shell SiO₂)

The core-shell silica microsphere templates were prepared using a slightly modified Stöber procedure.⁵³ In brief, 75 mL of ethanol, 10 mL of deionized water, and 3 mL of ammonia solution were added to a round-bottom flask, and the solution was stirred for 10 min. Using a syringe, TEOS (6 mL) was injected into the solution. After vigorous stirring for 2 h, a mixture of TEOS (5 mL) and C₁₈-TMS (2 mL) was added, and the solution was stirred for another 2 h. A white precipitate was formed and separated from the solution by centrifugation. To remove all organic residues in the precipitated powders, the powders were sintered in air at 550 °C for 6 h, yielding 2.0 g of silica powders. Silica has a spherical shape and a core-shell structure. The core diameter is approximately 300 nm and the shell thickness ranges from 20 to 30 nm.⁴²

Synthesis of hollow nickel-coated silica microspheres (Ni@SiO₂)

The prepared core-shell SiO₂ microspheres (0.495 g) were dispersed in 250 mL of deionized water in a 500 mL round-bottom flask. Nickel acetylacetonate (0.4 g, 1.6 × 10⁻³ mol) and urea (4.0 g, 6.7 × 10⁻² mol) were dissolved into the solution, which was then stirred at 80 °C for 2 h. The white microspheres gradually became green colloidal spheres, which were separated from the solution by centrifugation (3000 rpm), and dried in an oven at 100 °C. The dried microspheres (Ni(OH)₂@SiO₂) were

annealed at 750 °C for 20 h under a reducing atmosphere ($\text{Ar}/\text{H}_2 = 95 : 5$) to yield the desired nickel-coated microspheres.

Synthesis of hollow nickel-coated silica microspheres containing rhodium ($\text{Rh}/\text{Ni}@\text{SiO}_2$)

The procedure for the synthesis of $\text{Rh}/\text{Ni}@\text{SiO}_2$ is virtually identical to that of $\text{Ni}@\text{SiO}_2$ except that rhodium chloride hydrate is added as a source of Rh. The core-shell SiO_2 microspheres (0.495 g) were dispersed in 250 mL of deionized water in a 500 mL round-bottom flask. Rhodium chloride hydrate (0.04 g, 1.9×10^{-4} mol), nickel acetylacetonate (0.4 g, 1.6×10^{-3} mol), and urea (4.0 g, 6.7×10^{-2} mol) were dissolved into the solution, which was then stirred at 80 °C for 2 h. The white microspheres gradually became green colloidal spheres, which were separated from the solution by centrifugation (3000 rpm), and dried in an oven at 100 °C. The dried microspheres ($\text{Rh}/\text{Ni}(\text{OH})_2@\text{SiO}_2\text{-1T}$) were annealed at 750 °C for 20 h under a reducing atmosphere ($\text{Ar}/\text{H}_2 = 95 : 5$). The rhodium-deposited nickel-coated silica microspheres are denoted as $\text{Rh}/\text{Ni}@\text{SiO}_2\text{-1T}$. Prior to annealing, the dried microspheres were coated once more in a similar manner. The resulting microspheres were annealed at 750 °C for 20 h under a Ar/H_2 (95 : 5) atmosphere. These annealed microspheres are denoted as $\text{Rh}/\text{Ni}@\text{SiO}_2\text{-2T}$. Similarly, a $\text{Rh}/\text{Ni}@\text{SiO}_2\text{-3T}$ sample was prepared by repeating the procedure three times.

Hydrogen production from hydrous hydrazine

The evolution of hydrogen from hydrazine was examined using a two-necked round-bottom flask at room temperature; one neck was connected to a gas burette and the other neck was used to inject a solution of hydrazine hydrate. The catalyst ($\text{Rh}/\text{Ni}@\text{SiO}_2$, 50 mg) was loaded into the flask and dispersed in 5.0 mL of deionized water containing 1 mL of 0.5 M NaOH under an Ar atmosphere. Hydrazine hydrate (0.1032 g, 2.06 mmol) was then added to the catalyst *via* a syringe. Gas evolution was observed immediately. The gases released from the solution first passed through a trap containing sulfuric acid (0.1 M); this trap absorbed ammonia gas, which might be generated by the reaction. The amounts of passed gases were volumetrically measured using a gas burette. To determine the amounts of NH_3 and N_2H_4 left in the flask after the reaction, the indophenol-blue method was employed. Two solutions were prepared to perform this test. One solution comprised of 0.5 g of phenol and 2.83 mg of $\text{Na}_2[\text{Fe}(\text{CN})_5\text{NO}] \cdot 2\text{H}_2\text{O}$ in 50 mL of deionized water and the other comprised of 0.251 g of NaOH and 0.15 mL of NaOCl in 50 mL of deionized water. The pH of the solution that remained in the round-bottom flask was adjusted to 7.0 using a 0.1 M H_2SO_4 solution. Then, 1 mL of the pH-adjusted solution and 5 mL of each of the two solutions was mixed, and the resultant solution was stirred thoroughly for 1 h. The absorbance of the solution was measured and the total concentration was determined using a calibration curve obtained from a standard solution.^{54,55} In a similar manner, the amounts of NH_3 and N_2H_4 in the H_2SO_4 trap were also determined.

Methods

Powder X-ray diffraction (XRD) patterns were recorded using a Rigaku DMAX 2500 diffractometer (Cu $K\alpha$; Rigaku, Japan) operating at 40 kV and 150 mA. Transmission electron microscopy (TEM) was performed using a JEOL JEM-2100F microscope (JEOL, Japan). Specimens for TEM examinations were prepared by dispersing finely ground powders of the samples in anhydrous ethanol and then allowing a drop of the suspension to evaporate on a 400 mesh carbon-coated grid. Energy-dispersive X-ray (EDX) spectroscopy was performed using the same microscope as used for TEM. Line-scan analyses were performed in scanning transmission electron microscope-mode using a real-time interactive imaging system with a high-angle annular dark-field detector. Adsorption and desorption measurements were carried out at 77 K using an ASAP 2420 instrument (Micromeritics, Norcross, USA) with nitrogen as the adsorptive gas. The Brunauer–Emmett–Teller (BET) surface areas were calculated using the following: $P/P_0 = 0.05\text{--}0.3$ from the adsorption curve using the BET equation. The pore-size distributions were obtained from the desorption curve using the density functional theory method. Prior to each sorption measurement, the sample was out-gassed at 300 °C for 24 h *in vacuo* to completely remove the impurities. To investigate the elemental compositions, X-ray photoelectron spectroscopy (XPS; Theta probe AR-XPS System, Thermo Fisher Scientific, UK) analysis using a monochromated Al $K\alpha$ X-ray source ($h\nu = 1486.6$ eV) was performed at the Korea Basic Science Institute (KBSI) in Busan. Field emission scanning electron microscopy (FE-SEM) was performed using a Hitachi S-4700 microscope at KBSI in Jeonju. The contents of Ni and Rh in $\text{Rh}/\text{Ni}@\text{SiO}_2$ were analyzed using inductively coupled plasma atomic emission spectroscopy (ICP-AES, JY Ultima2C) at KBSI in Seoul.

Results and discussion

Our strategy to prepare hollow microspheres containing nickel hydroxide and rhodium species is illustrated in Fig. 1; this figure schematically represents the process for the synthesis of three different materials starting from core-shell SiO_2 microspheres: (a) yolk-shell microspheres with large yolks and thin shells, (b) yolk-shell microspheres with small yolks and thick shells, and (c) hollow microspheres with very thick shells. Our

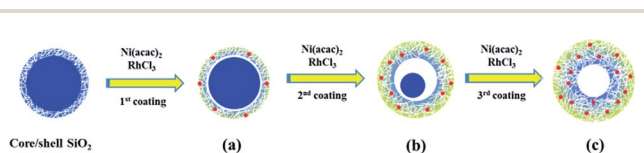


Fig. 1 Schematic representation of the preparation of hollow microspheres *via* the dissolution-and-deposition pathway using core-shell SiO_2 microspheres as templates: (a) $\text{Rh}/\text{Ni}(\text{OH})_2@\text{SiO}_2\text{-1T}$, (b) $\text{Rh}/\text{Ni}(\text{OH})_2@\text{SiO}_2\text{-2T}$, and (c) $\text{Rh}/\text{Ni}(\text{OH})_2@\text{SiO}_2\text{-3T}$. The cores and shells of the parent SiO_2 template are depicted in dark and light blue, respectively. Rh NPs are represented as red dots. The shells of (a), (b), and (c) are depicted in yellow and blue, which represent $\text{Ni}(\text{OH})_2$ and SiO_2 , respectively. The synthesis of $\text{Rh}/\text{Ni}(\text{OH})_2@\text{SiO}_2\text{-3T}$ involves three dissolution-and-deposition steps.

method relies on the thermal hydrolysis of urea to produce a hollow structure. The urea solution containing Rh and Ni precursors readily infiltrates into the silica template *via* mesopores in the shell. At 80 °C, urea dissociates into ammonium cations (NH_4^+) and hydroxide anions (OH^-) according to the following equation: $\text{NH}_2\text{CONH}_2 + 3\text{H}_2\text{O} \rightarrow \text{CO}_2 + 2\text{NH}_4^+ + 2\text{OH}^-$. The hydroxide anions generated from thermal hydrolysis of urea drive the ionization and dissolution processes on the SiO_2 surface. Deposition of Ni^{2+} and Rh^{3+} species appears to occur through electrostatic interactions on the ionized surface of SiO_2 . Metal species are presumably deposited on the silica shell in their hydroxide forms. Simultaneously, the silica cores gradually dissolve and form the inside of the silica shell. Repetition of this dissolution-and-deposition process eventually leads to the formation of hollow microspheres, which are composed of $\text{Ni}(\text{OH})_2$, SiO_2 , and Rh species. An important benefit of this method is that bimetallic hollow materials can be prepared simply by controlling the dissolution-and-deposition step.

Mavredaki *et al.* demonstrated that hydroxide ions promote the self-condensation of silicic acid in the pH range of 5–10 to yield dissolved silicate species.⁵⁶ Furthermore, this self-condensation process becomes more dominant when metal-hydroxide moieties are present on the SiO_2 surface. Tomiyama *et al.* also reported that nickel hydroxide particles on silica were prepared through deposition-and-precipitation processes.⁵⁷ These reported methods are straightforward; however, it is difficult to use them to achieve the desired shape and functionality. Our approach offers simple and convenient synthesis of hollow structures containing active metal species on the silica surface in a controlled manner. It is worth noting that the $\text{Rh}/\text{Ni}(\text{OH})_2@/\text{SiO}_2$ microspheres cannot be obtained using core SiO_2 microspheres with non-porous shells as templates; these microsphere templates yielded SiO_2 microspheres with irregular deposition of the metal species (Fig. S1†). These results clearly suggest that the porous shell also plays a crucial role in the dissolution-and-deposition processes. The cavity size and surface area can be tuned by adjusting the concentration of urea and heating temperature.

Typical TEM and SEM images of core-shell SiO_2 , $\text{Rh}/\text{Ni}(\text{OH})_2@/\text{SiO}_2$ -1T, $\text{Rh}/\text{Ni}(\text{OH})_2@/\text{SiO}_2$ -2T, and $\text{Rh}/\text{Ni}(\text{OH})_2@/\text{SiO}_2$ -3T are shown in Fig. 2 and demonstrate the distinctive changes in surface morphology after thermal hydrolysis of urea. The core-shell silica templates (Fig. 2(a)) had average diameters of 300 nm with shell thicknesses ranging from 20 to 30 nm. Fig. 2(b) shows a TEM image of $\text{Rh}/\text{Ni}(\text{OH})_2@/\text{SiO}_2$ -1T, which is the first dissolution-and-deposition product; this image clearly illustrates the formation of void space between the shell and core, which suggests that thermal hydrolysis of urea resulted in the slow dissolution of silica. Interestingly, the average diameter of $\text{Rh}/\text{Ni}(\text{OH})_2@/\text{SiO}_2$ -1T is slightly larger at ~ 340 nm. The void space increased in the second dissolution-and-deposition product, $\text{Rh}/\text{Ni}(\text{OH})_2@/\text{SiO}_2$ -2T, which had a clear yolk-shell structure. The TEM images shown in Fig. 2(c) reveal that the diameter of the yolk (core) was ~ 120 nm and the shell thickness drastically increased to about 60–80 nm; this suggests that the core silica gradually dissolved while the shell expanded through

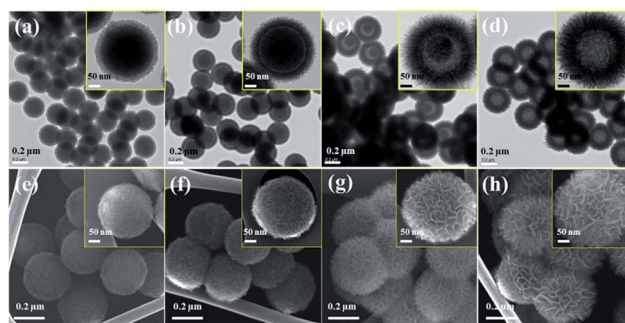


Fig. 2 Representative TEM images of (a) core-shell SiO_2 , (b) $\text{Rh}/\text{Ni}(\text{OH})_2@/\text{SiO}_2$ -1T, (c) $\text{Rh}/\text{Ni}(\text{OH})_2@/\text{SiO}_2$ -2T, and (d) $\text{Rh}/\text{Ni}(\text{OH})_2@/\text{SiO}_2$ -3T are displayed in the top panels. The bottom panels show SEM images of the corresponding samples, i.e., (e) core-shell SiO_2 , (f) $\text{Rh}/\text{Ni}(\text{OH})_2@/\text{SiO}_2$ -1T, (g) $\text{Rh}/\text{Ni}(\text{OH})_2@/\text{SiO}_2$ -2T, and (h) $\text{Rh}/\text{Ni}(\text{OH})_2@/\text{SiO}_2$ -3T. The insets show higher magnifications of the TEM and SEM images.

the deposition of dissolved silica as well as the $\text{Ni}(\text{OH})_2$ coating. As illustrated in Fig. 2(d), hollow microspheres with shell thicknesses of ~ 120 nm formed after three repeated reactions; this clearly demonstrates that the core is completely dissolved. The overall diameters of $\text{Rh}/\text{Ni}(\text{OH})_2@/\text{SiO}_2$ -3T ranged from 370 to 390 nm and were larger than that of the core-shell silica template. The TEM images suggest that dissolved silica accumulated inside the silica shell while the metal components were coated on the outer shell. This is in good agreement with the increment in diameter of the hollow microspheres.

Representative SEM images of the same samples are shown in the bottom panel of Fig. 2. The overall diameters of the samples were virtually identical to those estimated from the TEM images. The SEM images illustrate that the surface had a unique flower-like morphology. The flower-like surface becomes more distinctive with increasing number of dissolution-and-deposition steps. It has been reported that $\text{Ni}(\text{OH})_2$ grows in flower-like architectures in strongly alkaline solution. It is typically crystalline and shows distinctive XRD patterns corresponding to α - or β -phase $\text{Ni}(\text{OH})_2$. Interestingly, the XRD patterns of the as-prepared samples did not show any distinctive peaks (Fig. S2†), which suggests that all the phases in $\text{Rh}/\text{Ni}(\text{OH})_2@/\text{SiO}_2$ were amorphous. Thus far, an amorphous $\text{Ni}(\text{OH})_2$ phase with a flower-like morphology has not been reported. This amorphous nature suggests that the dissolved silica might interfere with the formation of a long-range ordered crystalline $\text{Ni}(\text{OH})_2$ phase. Instead, $\text{Ni}(\text{OH})_2$ petals grew along with dissolved silica species on the shell, which resulted in the formation of disordered amorphous $\text{Ni}(\text{OH})_2$. To investigate the elemental distribution and confirm the hollow structure, EDX line scan elemental profiles of the three $\text{Rh}/\text{Ni}(\text{OH})_2@/\text{SiO}_2$ samples were obtained as given in Fig. 3. The results confirm the presence of Ni, Si, and Rh, although the signal intensity of Rh is very low due to the minute amount of Rh in the sample. The EDX scan data clearly show that the intensity of Ni increases with increasing dissolution-and-deposition time while the intensity of Si decreases. In particular, the intensity of Si in the core is drastically reduced, confirming that the sample had a hollow structure. A notable feature in the line-

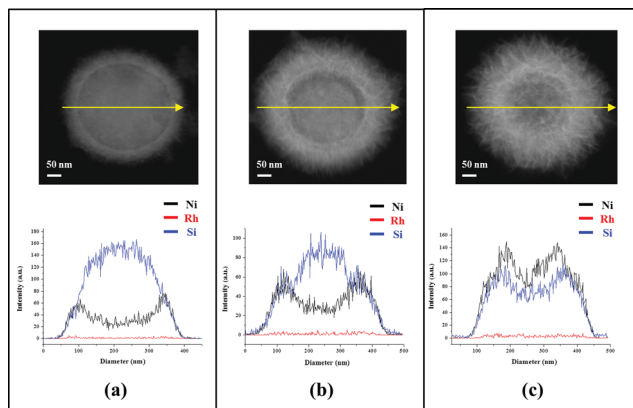


Fig. 3 EDX elemental line scans of (a) Rh/Ni(OH)₂@SiO₂-1T, (b) Rh/Ni(OH)₂@SiO₂-2T, and (c) Rh/Ni(OH)₂@SiO₂-3T. The top panels show the TEM images that include the positions of the line scan (yellow line). The bottom panel shows the EDS signal intensities of Ni, Si, and Rh across the diameter of the corresponding microsphere.

scan curves of Rh/Ni(OH)₂@SiO₂-3T is that the intensity of Ni is stronger than that of Si, which suggests that Ni(OH)₂ was predominantly coated on the outer shell while SiO₂ was mostly deposited on the inner shell. The EDX line-scan data are consistent with the TEM and SEM images shown in Fig. 2. The presence of Rh was not clear from the line-scan data but was confirmed by ICP-AES and EDX elemental analyses; this suggests that Rh species were embedded in the shell as tiny NPs. As evident from Table S1,[†] the two techniques yielded slightly different results because of their different measurement methods. We used the ICP-AES analysis data to evaluate the catalytic activity. With increasing dissolution-and-deposition time, the Rh content increased and was roughly proportional to the nominal composition. The maximum amount of Rh in Rh/Ni(OH)₂@SiO₂-3T was 6.35 wt%. In addition, the presence of Rh and the hollow structure were also evidenced by elemental mapping images shown in Fig. S7.[†]

To obtain crystalline bimetallic Rh/Ni phases, the Rh/Ni(OH)₂@SiO₂ samples were annealed at 750 °C for 20 h under flowing 5% H₂ in an Ar atmosphere, which converted them into hollow Rh/Ni@SiO₂ microspheres containing Ni and Rh NPs. As illustrated in the TEM images (Fig. 4), the parent hollow structures were maintained even after heating at high temperatures. Usually, annealing of hollow spheres composed of metal components at high temperatures leads to collapse or shrinkage of the parent hollow structure.^{58,59} However, in the case of Rh/Ni(OH)₂@SiO₂, the hollow shape was retained throughout the heat treatment because of the presence of silica layers in the inner shell, which appear to play a crucial role in maintaining the hollow structure. In addition, the silica layers act as supporting materials for the formation of the Ni layers. During the heating process, small amounts of the Rh species in the shells were deposited onto the abundant Ni surface to form bimetallic NPs. Relative to Rh/Ni(OH)₂@SiO₂-3T, the diameter of Rh/Ni@SiO₂-3T remained almost constant at 370 nm and the shell thickness ranged from 100 to 120 nm. Accordingly, the annealed sample retained the hollow structure with a virtually

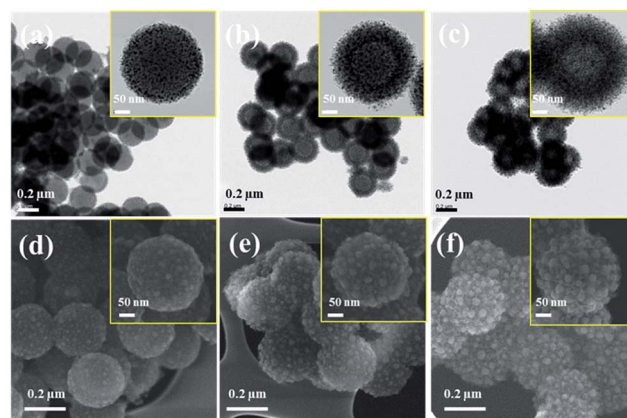


Fig. 4 The top panel shows TEM images of (a) Rh/Ni@SiO₂-1T, (b) Rh/Ni@SiO₂-2T, and (c) Rh/Ni@SiO₂-3T after heating the as-prepared samples at 750 °C under flowing 5% H₂ in an Ar atmosphere. The corresponding SEM images are illustrated in (d) Rh/Ni@SiO₂-1T, (e) Rh/Ni@SiO₂-2T, and (f) Rh/Ni@SiO₂-3T. The insets show higher magnifications.

identical shell thickness. However, annealing caused the flower-like surface morphology to disintegrate and large quasi-spherical agglomerates to grow along with the coated Ni layers. Thus, annealing transformed the flower-like Ni(OH)₂ phases into large metallic Ni granules and layers. This transformation process is quite similar to the melt-grown agglomeration procedure. The Ni(OH)₂ phase deposited on the outer shell melts at ~230 °C and the melted Ni particles initially coat on the surface. Some of the Ni phases agglomerate to form granules on the surface. In contrast, the extent of coarsening of the Rh species was limited, which is mainly because of their high melt temperature. The SEM images show that large Ni granules with spherical shapes protruded from the Ni surface (Fig. 4).

The structures of the bimetallic phases in the shell were characterized by XRD. As illustrated in Fig. 5, XRD patterns of the three Rh/Ni@SiO₂ samples show two distinctive peaks at 44.2 and 52.4°, which are typical of the Ni phase (space group: *Fm3m*) with a face-centered cubic structure (JCPDS no. 70-1849).⁶⁰⁻⁶³ The two peaks were assigned to the (111) and (200) reflections. A very broad peak near 20° was assigned to SiO₂ (JCPDS no. 29-0085). No diffraction peaks corresponding to Rh appeared even in Rh/Ni@SiO₂-3T, which indicates that the amount of Rh in the sample was too small to be detected by XRD.^{64,65} Another plausible scenario is that Rh alloyed with Ni to yield a Ni-rich bimetallic phase. The XRD data provide indirect evidence of the formation of bimetallic NPs. Namely, a part of the Rh metal was incorporated in the Ni metal to form alloy NPs while the remainder was present in the shell as sub-nanometer Rh NPs. This conjecture is also supported by the XRD patterns of Rh@SiO₂, which is shown in Fig. S6.[†]

The oxidation states and chemical environments of Rh, Ni, Si, and O in Rh/Ni@SiO₂-1T, Rh/Ni@SiO₂-2T, and Rh/Ni@SiO₂-3T were further characterized by XPS. Fig. S3[†] shows detailed XPS spectra of the important regions (*i.e.*, Rh 3d, Ni 2p, Si 2p, and O 1s) for each element. All species of interest are displayed in the XPS spectra. The Rh 3d signals are observed at 306 and

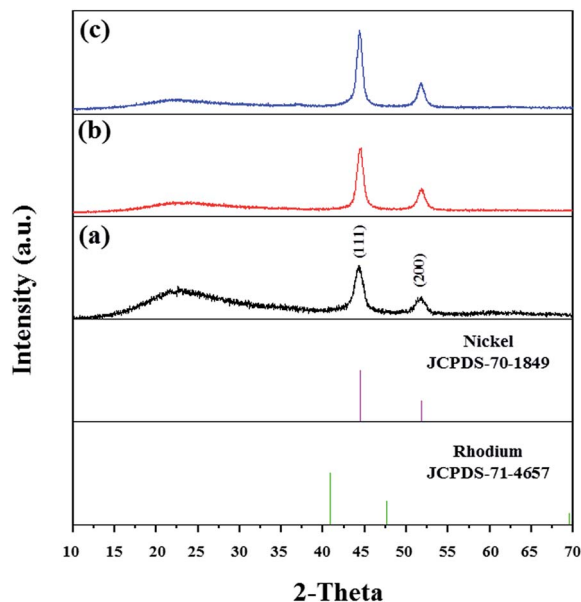


Fig. 5 Powder XRD patterns of (a) Rh/Ni@SiO₂-1T, (b) Rh/Ni@SiO₂-2T, and (c) Rh/Ni@SiO₂-3T. Theoretical XRD patterns of Ni and Rh are also displayed for reference.

310 eV, which were assigned to Rh 3d_{5/2} and Rh 3d_{3/2}, respectively. The two Rh 3d signals in Rh/Ni@SiO₂-3T are substantially more intense than those of Rh/Ni@SiO₂-1T, suggesting that the Rh/Ni@SiO₂-3T sample contained more Rh. Assignments of the Ni 2p peaks are complicated due to the presence of several Ni species in different chemical environments. Four peaks are displayed at ~857.2, 861.1, 874.8 and 879.7 eV. On the basis of previous reports on Ni metal, the two peaks at 857.2 and 874.8 eV were assigned to Ni 2p_{3/2} and Ni 2p_{1/2}, respectively.^{66–73} The two broad remaining peaks are presumably associated with NiO or could be ascribed to the satellite peak. The presence of characteristic Ni 2p signals in the Ni 2p XPS spectra indicates that metallic Ni was coated on the outer shell and NiO formed presumably at the boundary between Ni and SiO₂. The binding energies of Si 2p and O 1s are very close to the values reported for a range of silicate species.^{74–76}

Prior to testing the catalytic activities of Rh/Ni@SiO₂-1T, Rh/Ni@SiO₂-2T, and Rh/Ni@SiO₂-3T, we measured their N₂ adsorption and desorption isotherms to estimate their surface areas and pore sizes. Type-IV isotherm curves with distinctive hysteresis loops were observed for all three samples (Fig. S4†), which suggests the presence of mesopores in the shells.^{77–81} The specific surface areas of the samples were very high and quite similar, ranging from 172.63 to 180.21 m² g⁻¹. However, the pore-size distribution curves show that the pore sizes increased substantially from 4.7 nm in Rh/Ni@SiO₂-1T to 5.6 nm in Rh/Ni@SiO₂-3T. In addition, Rh/Ni@SiO₂-3T had a considerable number of pores that are 10 nm or larger. This suggests that a greater variety of pores sizes were produced with increasing number of dissolution-and-deposition steps.

Because of the high specific surface area of the bimetallic Rh/Ni@SiO₂ samples, they were expected to show great promise catalytically. Hydrous hydrazine was selected as a substrate to

illustrate the selective production of H₂ and N₂. To determine the efficiency of H₂ production using the bimetallic catalyst, we reacted hydrous hydrazine (0.404 M) with the catalyst at 25 °C in a round-bottom flask and measured the production of H₂ volumetrically using a gas burette. To ensure that the catalyst surface was basic and to prevent the production of unwanted NH₃ gas, NaOH (0.5 M) was added to the hydrazine solution. When Rh/Ni@SiO₂-1T was used as a catalyst, gases evolved for approximately 3.3 h and the amount of gases released over the course of the reaction was 2.77 equivalents (equiv.), as illustrated in Fig. 6. This corresponds to a H₂ selectivity of 91.3%. The turnover number (TON) of Rh/Ni@SiO₂-1T was about 143, which was calculated on the basis of the Rh content. Under the same reaction conditions, the second catalyst (Rh/Ni@SiO₂-2T) yielded 2.78 equiv. of gases in 1.6 h and had a 91.4% H₂ selectivity (TON = 90). The catalytic activity of Rh/Ni@SiO₂-3T towards the same reaction was also tested. Almost complete conversion of hydrazine was achieved in 1.5 h, yielding 2.99 equiv. of gases (TON = 66). The selectivity of Rh/Ni@SiO₂-3T toward H₂ production was remarkably high (99.4%). These results suggest that increasing the Rh content in the Rh/Ni@SiO₂ catalyst increases the H₂ selectivity as well as the yield. The optimal amount of Rh in the Ni-coated hollow catalyst was ~6.36 wt%, which is remarkably low compared with the values reported previously.³⁶ In a recent paper by Singh and Xu, it was demonstrated that the H₂ selectivity strongly depends on the Rh/Ni ratio in Rh_xNi_y alloys, and the Rh₄Ni catalyst with 87.5 wt% Rh reaches a maximum H₂ selectivity close to 100%. Thus, Rh/Ni@SiO₂-3T could be the catalyst with the lowest Rh content for the selective decomposition of hydrous hydrazine. Its high selectivity at low Rh loadings is unprecedented in RhNi alloys.

For comparison, monometallic catalysts that contain only Ni or Rh, such as Ni@SiO₂ and Rh@SiO₂, were used as catalysts under the same conditions. As illustrated in Fig. 7, no gas products were obtained when Ni@SiO₂ was used as a catalyst. Even over Rh@SiO₂ catalysts, a low yield and medium selectivity of 1.3 equiv. and 42%, respectively, were observed. Moreover, the release of gases terminated after about 6.3 h. These results

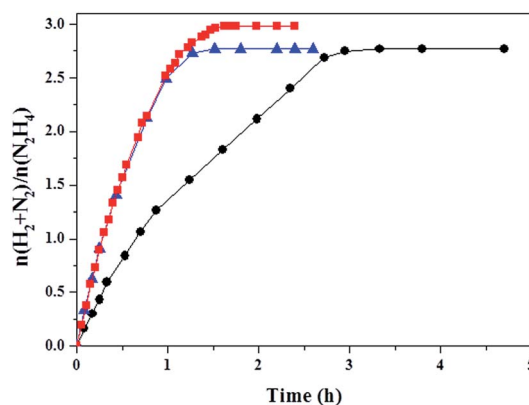


Fig. 6 Production of H₂ and N₂ from hydrous hydrazine as a function of time in the presence of NaOH (0.5 M) at 25 °C using Rh/Ni@SiO₂-1T (black circles), Rh/Ni@SiO₂-2T (blue triangles), and Rh/Ni@SiO₂-3T (red squares) catalysts.

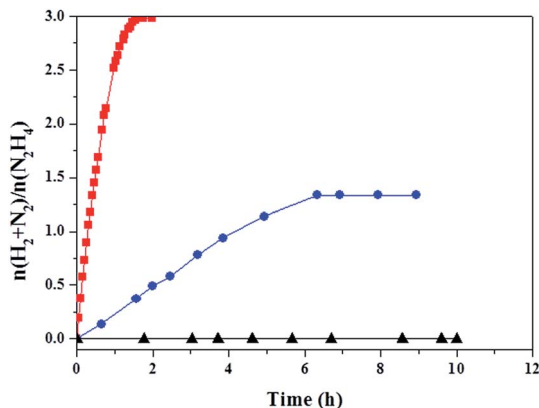


Fig. 7 Production of H₂ and N₂ from hydrous hydrazine as a function of time in the presence of NaOH (0.5 M) at 25 °C using Ni@SiO₂ (black triangles), Rh@SiO₂ (blue circles), and Rh/Ni@SiO₂-3T (red squares) catalysts.

clearly demonstrate that the bimetallic alloy is crucial for high yield and selectivity. The RhNi bimetallic species anchored on the Ni surface appear to promote the adsorption of hydrous hydrazine so that complete decomposition of hydrous hydrazine into H₂ and N₂ predominantly occurs. Thus, the bimetallic hollow catalysts (Rh/Ni@SiO₂) clearly show a synergetic effect and superior catalytic activity compared to those of the mono-metallic congeners. Table S2† presents an overview of recently reported catalysts that efficiently produced hydrogen from hydrous hydrazine. Compared with other Rh alloy catalysts (entries 3 and 9), the Rh/Ni@SiO₂ catalyst shows excellent H₂ selectivity even at 25 °C despite the low Rh content.

Because of the presence of magnetic Ni layers in the Rh/Ni@SiO₂ microsphere, the catalyst was separated simply by using a magnet after completion of the reaction (Fig. S5†). A remarkable advantage of these catalysts is that they can be reused without loss of catalytic activity. The Rh/Ni@SiO₂-3T catalyst was recycled three times; the results are shown in Fig. 8.

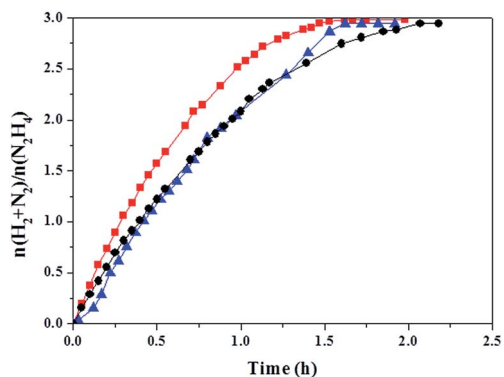


Fig. 8 Recycle test of the Rh/Ni@SiO₂-3T catalyst: production of H₂ and N₂ from hydrous hydrazine as a function of time in the presence of NaOH (0.5 M) at 25 °C using a Rh/Ni@SiO₂-3T catalyst. The red squares, blue triangles, and black circles indicate the first, second, and third cycles, respectively. The used catalysts were separated by using a magnet after the reaction.

For the second cycle, the reaction provided a virtually identical yield of gases (2.99 equiv.). Even for the third cycle, the yield of gases released was 2.99 equiv. although the reaction took slightly longer (2.0 h) than the first run. These results clearly demonstrate that the bimetallic NPs supported on hollow Ni-coated microspheres are highly resistant to deactivation in alkaline solution and retain excellent catalytic activity for the complete decomposition of hydrous hydrazine. Thus, hollow Rh/Ni@SiO₂-3T microspheres can be considered to be one of the most promising catalysts for hydrogen production from hydrous hydrazine in commercial applications.

Conclusions

In conclusion, we developed a simple and efficient methodology for the synthesis of hollow Ni-coated microspheres (Rh/Ni@SiO₂) containing Rh NPs using core-shell silica microspheres as templates. The Ni-coated hollow microsphere with a low loading of Rh showed excellent catalytic performance for complete conversion of NH₂NH₂ into H₂ and N₂ at room temperature with over 99% H₂ selectivity. Our study highlights a method for the exclusive production of H₂ from NH₂NH₂ using a low-cost and recyclable catalyst under industrially realistic conditions, which opens up the possibility of accelerating the practical application of H₂NNH₂ as a hydrogen-storage material.

Acknowledgements

This work was supported by the Korea CCS R&D Center Grant funded by the Korea government (Ministry of Science, ICT & Future Planning, 2013M1A8A1035853). BL thanks the Research Fellow Program (2012R1A12043256).

Notes and references

- 1 Y. Xia, Z. Yang and Y. J. Zhu, *J. Mater. Chem. A*, 2013, **1**, 9365.
- 2 K. Shimura and H. Yoshida, *Energy Environ. Sci.*, 2011, **4**, 2467.
- 3 L. Schlapbach and A. Züttel, *Nature*, 2001, **414**, 353.
- 4 N. Armaroli and V. Balzani, *ChemSusChem*, 2011, **4**, 21.
- 5 J. B. O. Santos, G. P. Valenca and J. A. J. Rodrigues, *J. Catal.*, 2002, **210**, 1.
- 6 B. Sakintuna, F. Lamari-Darkrim and M. Hirscher, *Int. J. Hydrogen Energy*, 2007, **32**, 1121.
- 7 G. Moussa, R. Moury, U. Demirci, T. Sener and P. Miele, *Int. J. Energy Res.*, 2013, **37**, 825.
- 8 D. Teichmann, W. Arlt, P. Wasserscheid and R. Freymann, *Energy Environ. Sci.*, 2011, **4**, 2767.
- 9 L. Chong, J. Zou, X. Zeng and W. Ding, *J. Mater. Chem. A*, 2013, **1**, 3983.
- 10 S. S. Muir and X. Yao, *Int. J. Hydrogen Energy*, 2011, **36**, 5983.
- 11 J. Zhang, T. S. Fisher, J. P. Gore, D. Hazra and P. V. Ramachandran, *Int. J. Hydrogen Energy*, 2006, **31**, 2292.
- 12 H. Dai, Y. Liang, L. Ma and P. Wang, *J. Phys. Chem. C*, 2008, **112**, 15886.

- 13 H. I. Schlesinger, H. C. Brown, A. E. Finholt, J. R. Gilbreath, H. R. Hoekstra and E. K. Hyde, *J. Am. Chem. Soc.*, 1953, **75**, 215.
- 14 B. H. Liu and Z. P. Li, *J. Power Sources*, 2009, **187**, 527.
- 15 M. J. F. Ferreira, L. Gales, V. R. Fernandes, C. M. Rangel and A. M. F. R. Pinto, *Int. J. Hydrogen Energy*, 2010, **35**, 9869.
- 16 S. J. Cho, J. Lee, Y. S. Lee and D. P. Kim, *Catal. Lett.*, 2006, **109**, 181.
- 17 S. K. Singh and Q. Xu, *Catal. Sci. Technol.*, 2013, **3**, 1889.
- 18 H. Jiang, S. K. Singh, J. Yan, X. Zhang and Q. Xu, *ChemSusChem*, 2010, **3**, 541.
- 19 D. G. Tong, W. Chu, P. Wu, G. F. Gu and L. Zhang, *J. Mater. Chem. A*, 2013, **1**, 358.
- 20 E. W. Schmidt, *Hydrazine and its Derivatives: Preparation, Properties, Applications*, John Wiley and Sons, Inc., 2nd edn, 2001, vol. 1–2.
- 21 L. He, Y. Huang, X. Y. Liu, L. Li, A. Wang, X. Wang, C. Mou and T. Zhang, *Appl. Catal., B*, 2014, **147**, 779.
- 22 K. V. Manukyan, A. Cross, S. Rouvimov, J. Miller, A. S. Mukasyan and E. E. Wolf, *Appl. Catal., A*, 2014, **476**, 47.
- 23 T. Umegaki, J. Yan, X. Zhang, H. Shioyama, N. Kuriyama and Q. Xu, *Int. J. Hydrogen Energy*, 2009, **34**, 2303.
- 24 A. K. Singh and Q. Xu, *Int. J. Hydrogen Energy*, 2014, **39**, 9128.
- 25 L. He, Y. Huang, A. Wang, X. Wang, X. Chen, J. J. Delgado and T. Zhang, *Angew. Chem., Int. Ed.*, 2012, **51**, 6191.
- 26 L. He, Y. Huang, A. Wang, X. Wang and T. Zhang, *AIChE J.*, 2013, **59**, 4297.
- 27 L. He, Y. Huang, A. Wang, Y. Liu, X. Liu, X. Chen, J. J. Delgado, X. Wang and T. Zhang, *J. Catal.*, 2013, **298**, 1.
- 28 M. Yadav and Q. Xu, *Energy Environ. Sci.*, 2012, **5**, 9698.
- 29 S. K. Singh, X. Zhang and Q. Xu, *J. Am. Chem. Soc.*, 2009, **131**, 9894.
- 30 S. K. Singh and Q. Xu, *Chem. Commun.*, 2010, **46**, 6545.
- 31 S. K. Singh, Z. Lu and Q. Xu, *Eur. J. Inorg. Chem.*, 2011, **2011**, 2232.
- 32 J. Zhang, Q. Kang, Z. Yang, H. Dai, D. Zhuang and P. Wang, *J. Mater. Chem. A*, 2013, **1**, 11623.
- 33 S. K. Singh, Y. Iizuka and Q. Xu, *Int. J. Hydrogen Energy*, 2011, **36**, 11794.
- 34 S. K. Singh, A. K. Singh, K. Aranishi and Q. Xu, *J. Am. Chem. Soc.*, 2011, **133**, 19638.
- 35 D. G. Tong, D. M. Tang, W. Chu, G. F. Gu and P. Wu, *J. Mater. Chem. A*, 2013, **1**, 6425.
- 36 S. K. Singh and Q. Xu, *J. Am. Chem. Soc.*, 2009, **131**, 18032.
- 37 A. K. Singh, M. Yadav, K. Aranishi and Q. Xu, *Int. J. Hydrogen Energy*, 2012, **37**, 18915.
- 38 J. Wang, X. Zhang, Z. Wang, L. Wang and Y. Zhang, *Energy Environ. Sci.*, 2012, **5**, 6885.
- 39 C. Yan and D. Xue, *J. Phys. Chem. B*, 2006, **110**, 7102.
- 40 X. W. Lou, L. A. Archer and Z. Yang, *Adv. Mater.*, 2008, **20**, 3987.
- 41 X. Gong, L. Wang and W. Wen, *Chem. Commun.*, 2009, 4690.
- 42 J. B. Yoo, H. J. Yoo, B. W. Lim, K. H. Lee, M. H. Kim, D. Kang and N. H. Hur, *ChemSusChem*, 2012, **5**, 2334.
- 43 E. Hemmer, N. Venkatachalam, H. Hyodo, A. Hattori, Y. Ebina, H. Kishimoto and K. Soga, *Nanoscale*, 2013, **5**, 11339.
- 44 C. Chen, L. K. Yee, H. Gong, Y. Zhang and R. Xu, *Nanoscale*, 2013, **5**, 4314.
- 45 W. Di, S. K. P. Velu, A. Lascialfari, C. Liu, N. Pinna, P. Arosio, Y. Sakka and W. Qin, *J. Mater. Chem.*, 2012, **22**, 20641.
- 46 Z. Xu, Y. Gao, T. Liu, L. Wang, S. Bian and J. Lin, *J. Mater. Chem.*, 2012, **22**, 21695.
- 47 Z. H. Zhang, L. Chen, Q. H. Gan, Q. Tian, C. L. Chen and Z. L. Huang, *Phys. Status Solidi A*, 2013, **210**, 378.
- 48 H. Qin, X. Zhang, H. Liu, Y. Sang and J. Wang, *CrystEngComm*, 2013, **15**, 5076.
- 49 L. Su, C. Ma, T. Hou and W. Han, *RSC Adv.*, 2013, **3**, 19807.
- 50 P. Burattin, M. Che and C. Louis, *J. Phys. Chem. B*, 1997, **101**, 7060.
- 51 M. Khoudiakov, M. C. Gupta and S. Deevi, *Appl. Catal., A*, 2005, **291**, 151.
- 52 J. A. Schwarz, *Chem. Rev.*, 1995, **95**, 477.
- 53 W. Stöber and A. Fink, *J. Colloid Interface Sci.*, 1968, **26**, 62.
- 54 T. T. Ngo, A. P. H. Phan, C. F. Yam and H. M. Lenhoff, *Anal. Chem.*, 1982, **54**, 46.
- 55 P. Moreno, E. Sánchez, A. Pons and A. Palou, *Anal. Chem.*, 1986, **58**, 585.
- 56 E. Mavredaki, E. Neofotistou and K. D. Demadis, *Ind. Eng. Chem. Res.*, 2005, **44**, 7019.
- 57 S. Tomiyama, R. Takahashi, S. Sato, T. Sodesawa and S. Yoshida, *Appl. Catal., A*, 2003, **241**, 349.
- 58 R. Nakamura and H. Nakajima, *J. Phys.: Conf. Ser.*, 2009, **165**, 012072.
- 59 R. Nakamura, D. Tokozakura, J. Lee, H. Mori and H. Nakajima, *Acta Mater.*, 2008, **56**, 5276.
- 60 J. Gao, C. Jia, M. Zhang, F. Gu, G. Xu and F. Su, *Catal. Sci. Technol.*, 2013, **3**, 2009.
- 61 A. Jangam and S. Kawi, *ACS Catal.*, 2014, **4**, 289.
- 62 S. Wang, X. Guo, H. Yang, J. Dai, R. Zhu, J. Gong, L. Peng and W. Ding, *Appl. Surf. Sci.*, 2014, **288**, 530.
- 63 Y. Luo, J. Zhang, Y. Shen, S. Jiang and G. Liu, *J. Mater. Sci. Technol.*, 2007, **5**, 587.
- 64 H. Jiang, T. Umegaki, T. Akita, X. Zhang, M. Haruta and Q. Xu, *Chem.–Eur. J.*, 2010, **16**, 3132.
- 65 K. S. Han and O. H. Han, *Bull. Korean Chem. Soc.*, 2006, **26**, 1121.
- 66 Y. Hou and S. Gao, *J. Alloys Compd.*, 2004, **365**, 112.
- 67 F. Liu, J. Y. Lee and W. Zhou, *J. Phys. Chem. B*, 2004, **108**, 17959.
- 68 A. P. Grosvenor, M. C. Biesinger, R. St. C. Smart and N. S. McIntyre, *Surf. Sci.*, 2006, **600**, 1771.
- 69 L. Xia, X. Hu, X. Kang, H. Zhao, M. Sun and X. Cihen, *Colloids Surf., A*, 2010, **367**, 96.
- 70 H. B. Li, M. H. Yu, F. X. Wang, P. Liu, Y. Liang, J. Xiao, C. X. Wang, Y. X. Tong and G. W. Yang, *Nat. Commun.*, 2013, **4**, 1894.
- 71 L. Mi, Q. Ding, W. Chen, L. Zhao, H. Hou, C. Liu, C. Shen and Z. Zheng, *Dalton Trans.*, 2013, **42**, 5724.
- 72 Z. Xu, J. Yu, G. Liu, B. Cheng, P. Zhou and X. Li, *Dalton Trans.*, 2013, **42**, 10190.
- 73 J. Yang, X. Duan, Q. Qin and W. Zheng, *J. Mater. Chem. A*, 2013, **1**, 7880.

- 74 G. He, G. W. Meng, L. D. Zhang and M. Liu, *Appl. Phys. Lett.*, 2007, **91**, 232910.
- 75 S. N. Arafat, S. Dutta, M. Perring, M. Mitchell, P. J. A. Kenis and N. B. Bowden, *Chem. Commun.*, 2005, 3198.
- 76 T. D. Shen, I. Shmagin, C. C. Koch, R. M. Kolbas, Y. Fahmy, L. Bergman, R. J. Nemanich, M. T. McClure, Z. Sitar and M. X. Quan, *Phys. Rev. B: Condens. Matter Mater. Phys.*, 1997, **55**, 7615.
- 77 H. Lin, S. Wong, C. Mou and C. Tang, *J. Phys. Chem. B*, 2000, **104**, 8967.
- 78 J. Li, J. Lin, X. Xu, X. Zhang, Y. Xue, J. Mi, Z. Mo, Y. Fan, L. Hu, X. Yang, J. Zhang, F. Meng, S. Yuan and C. Tang, *Nanotechnology*, 2013, **24**, 155603.
- 79 R. Jia, J. Chen, J. Zhao, J. Zheng, C. Song, L. Li and Z. Zhu, *J. Mater. Chem.*, 2010, **20**, 10829.
- 80 Y. Liang, D. Wu and R. Fu, *Sci. Rep.*, 2013, **3**, 1119.
- 81 S. Feng, W. Li, Q. Shi, Y. Li, J. Chen, Y. Ling, A. M. Asiri and D. Zhao, *Chem. Commun.*, 2014, **50**, 329.